Journal of
Micromechanics and
Microengineering

TECHNICAL NOTE

Mechanical characterization of polydimethylsiloxane (PDMS) exposed to thermal histories up to 300 °C in a vacuum environment

To cite this article: Derya Z Tansel *et al* 2020 *J. Micromech. Microeng.* **30** 067001

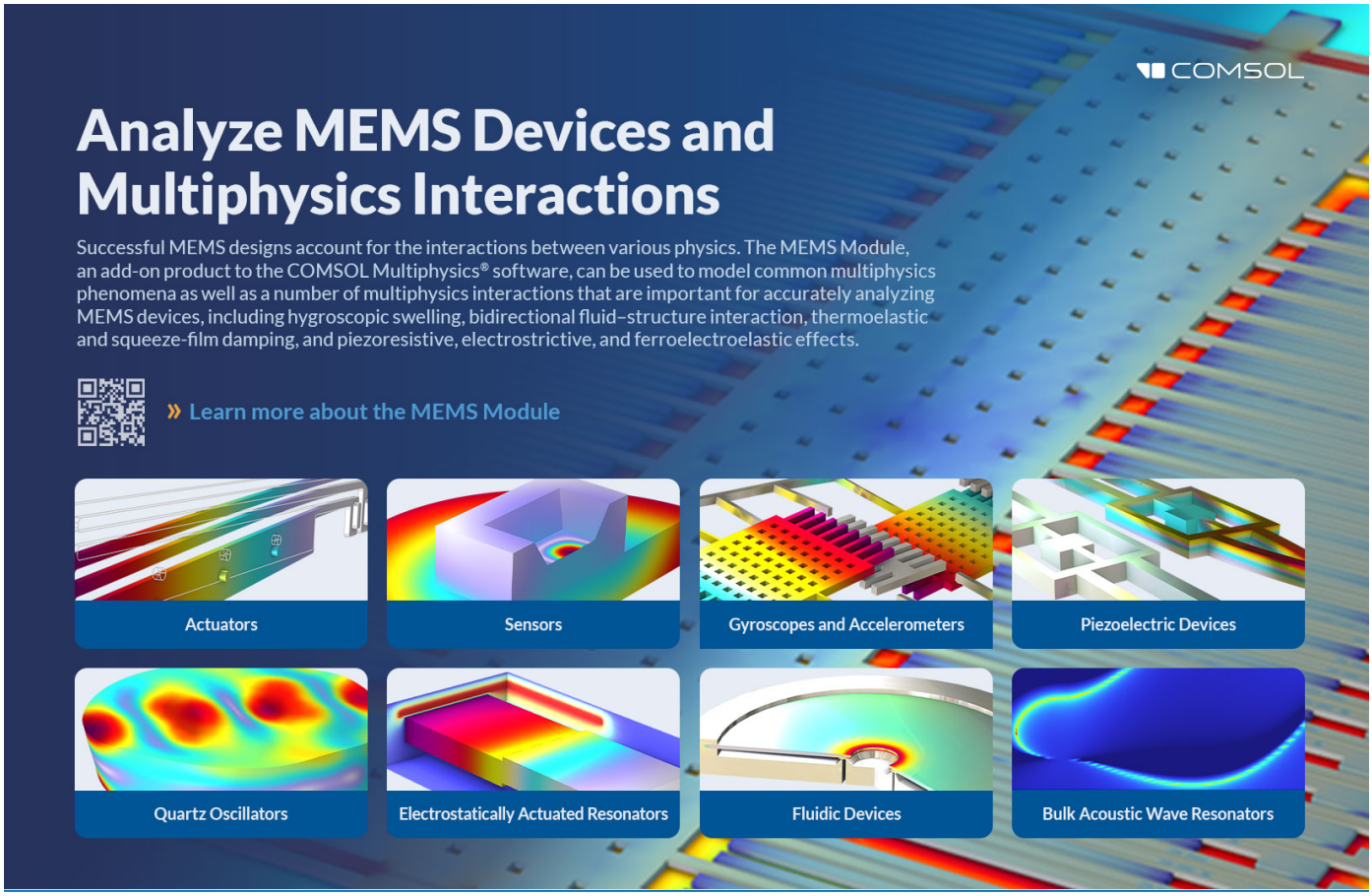

IOP Publishing Journal of Micromechanics and Microengineering
J. Micromech. Microeng. **30** (2020) 067001 (7pp) https://doi.org/10.1088/1361-6439/ab82f4

Technical Note

Mechanical characterization of polydimethylsiloxane (PDMS) exposed to thermal histories up to 300 °C in a vacuum environment

Derya Z Tansel[1], Jacob Brenneman[2], Gary K Fedder[1,2,3] and Rahul Panat[2]

[1] Department of Electrical and Computer Engineering, Carnegie Mellon University, Pittsburgh, PA 15213, United States of America
[2] Department of Mechanical Engineering, Carnegie Mellon University, Pittsburgh, PA 15213, United States of America
[3] Robotics Institute, Carnegie Mellon University, Pittsburgh, PA 15213, United States of America

E-mail: rpanat@andrew.cmu.edu and fedder@cmu.edu

Received 2 February 2020, revised 16 March 2020
Accepted for publication 24 March 2020
Published 28 April 2020

Abstract

Flexible electronic devices consisting of sensors and interconnects integrated with a soft polymer platform are being considered for emerging applications such as smart clothing, soft robotics, conformal batteries, and biomonitoring decals. Fabrication processes for such devices can require that the polymer platform be subjected to temperatures up to 300 °C without a significant deterioration of its physical properties such as stretchability and stiffness. In this communication, we report the stress–strain behavior of relatively thin sheets of polydimethylsiloxane (PDMS) polymer (thickness ∼30 μm) made with a base-to-hardener ratio of 20:1 and heated up to 300 °C in a vacuum environment. It is shown that in spite of the exposure to high temperatures used in this study, the PDMS sheets maintained their hyperelastic behavior as represented by the Ogden model. The elastic modulus is shown to decrease from 0.81 MPa to 0.62 MPa while average strain to failure is shown to decrease from 250% to 106% as the temperature of thermal exposure in vacuum is increased from 100 °C to 300 °C. The retention of high stretchability even after the thermal exposures opens up the possibility of high-density microelectronic circuit interconnects to be fabricated on PDMS substrates.

Supplementary material for this article is available online

Keywords: PDMS, flexible electronics, thermal history, hyperelasticity models, Ogden model, microelectronics manufacturing

(Some figures may appear in colour only in the online journal)

1. Introduction

Polydimethylsiloxane (PDMS) is a silicon-based organic polymer used in a wide variety of applications such as microfluidics, cosmetics, and biomedicine. Recently, PDMS has been considered as a substrate material for flexible electronic devices due to its biocompatibility, sub-micron resolution, leak-proof packaging, and resistance to weathering [1–5]. Further, PDMS exhibits a high stretchability (>100%) and flexibility that is well above that of the skin (∼30%), making it

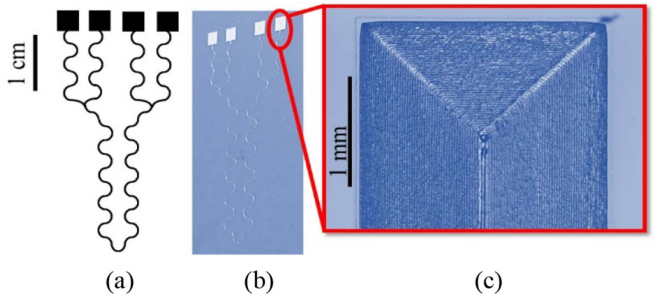

Figure 1. Aerosol-jet printed (AJP) circuit comprising silver nanoparticles on 20:1 PDMS and sintered at 300 °C for 3 h. (a) Layout. (b) Optical micrograph. (c) Magnified micrograph of AJP pad.

an ideal candidate for wearable biomonitoring devices [3, 6]. The properties of as-made PDMS can be further modulated by changing the mixing ratios of its base elastomer to curing agent from 5:1 to 33:1 [7].

Polymer substrates used in microelectronic circuits can be heated to temperatures as high as 250 to 300 °C during the fabrication or packaging processes. These temperatures are required for flip-chip bonding, solder-ball attaching, or interconnect formation via sintering of nanoparticles deposited by methods such as aerosol jet or inkjet printing on rigid or flexible printed-circuit boards [8, 9].

Electrically conductive inks, such as nanoparticle silver inks, are directly printed on polymers to create stretchable electronic devices [10, 11]. However, the nanoparticle sintering temperature is as high as 250 to 300 °C [12], which precludes the use of several polymers for printing application. Methods such as photonic sintering [13, 14] and localized low-power laser sintering [14] have been developed to overcome this problem, but they need to be optimized for particular material sets. An example of high temperature microelectronics fabrication in our efforts is shown in figure 1, where a silver nanoparticle circuit is printed using an aerosol-jet 3D printing method on 20:1 PDMS and subjected to 3 h of sintering at 300 °C in vacuum.

The ability to subject PDMS polymer to the process temperatures used in microelectronics manufacturing would allow a significant flexibility in the types of electronic circuits and functionalities that can be integrated with devices that use PDMS as the substrate material [10]. Note that PDMS is expected to undergo thermal degradation at high temperatures through the formation of Si-O bonds (oxidation), which is accelerated in the presence of heat and oxygen [15, 16]. A study of the evolution of volatile materials from PDMS showed that the presence of oxygen indeed accelerated its degradation at high temperatures [15, 16].

The mechanical properties of PDMS have been measured in literature for different cure times, thicknesses, and strain rates [17–21], including a comparison for various mixing ratios of PDMS base to curing agent [18, 19]. These studies show that the Young's modulus (i.e. stiffness) of PDMS increases with a decrease in mixing ratio, a decrease in thickness, and an increase in the strain rate [17–19]. These reports of PDMS properties, however, have been limited to the low strain elastic region [20, 21]. The behavior of PDMS films in tension has also been modeled by assuming an incompressible hyperelastic material behavior utilizing both the Ogden [22] and Mooney-Rivlin models [23] fit to data in stress vs strain plots [24, 25]. A variety of other hyperelastic models exist, including the Neo-Hookean [26] and Yeoh [27] models, but much of the existing data analyzed at high strains for PDMS is focused on the Mooney–Rivlin and Ogden models. Furthermore, both the Ogden model and Mooney–Rivlin models were used to fit data shown in this work, and the Ogden model was determined to fit the data more closely and thus chosen to report mechanical properties.

The impetus for the present work was two-fold. First, we aimed to gain a comprehensive understanding of the changes in stiffness and strain-to-failure (two properties most important to applications such as flexible electronics) of PDMS films with a 20:1 mixing ratio exposed to high temperatures at low vacuum (∼1 Torr). The focus was to subject the PDMS to thermal histories mimicking those in the microelectronics manufacturing processes. Second, we wanted to use mechanical modeling to gain an insight into the possible degradation of the films under different thermal histories. The focus was on using hyperelasticity models to fit the experimental data to measure and quantify the degradation in mechanical behavior.

2. Experimental

2.1. PDMS fabrication

The PDMS samples (Sylgard 184, Dow Corning Corporation, Midland, MI), were fabricated by mixing the base (prepolymer) and the curing agent (cross-linker) of the polymer at ratios of 20:1. In an initial feasibility test, a handful of 10:1 specimens (the manufacturer's recommended mix ratio) cured at 300 °C in vacuum were very brittle and broke, while 20:1 specimens showed promising characteristics. One set of 10:1 specimens cured at 100 °C was added to the experimental protocol as a baseline comparison to results found in literature [17, 28, 29]. The mixtures were degassed for 30 min to remove bubbles. The PDMS mixtures were then spin-cast for 60 s at 500 rpm followed by 120 s at 1000 rpm to get 27−35 μm thick films on a Si wafer coated with polyacrylic acid (PAA) used as a sacrificial release layer (see figure 2). All PDMS specimens were initially cured at 100 °C in atmospheric conditions. Some of the specimens were then treated in a nitrogen vented vacuum chamber for 1 h at 1 Torr for temperatures of 100 °C, 200 °C, and 300 °C. Table 1 provides the different conditions applied to the PDMS samples. Four samples were tested for each condition. Specimens were cut using a sharp cutter (Curio™, Silhouette America, Lindon, UT, USA) and released in saline overnight to dissolve the PAA. Thickness for all of the PDMS samples was measured with a surface profilometer (Dektak 3, Bruker Corporation, Billerica, MA). An aperture card was used to handle each specimen to ensure its smooth insertion in the tensile testing machine.

2.2. Stretching experiments and modeling

PDMS specimens were cut to a modified type-C specimen shape described in ASTM D412 [30] with dimensions as

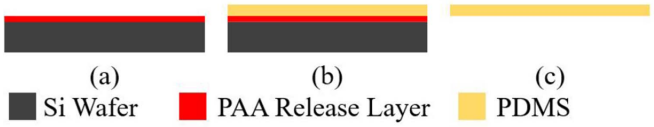

Figure 2. Fabrication flow of the specimens: (a) spin coating of PAA (polyacrylic acid) release layer; (b) spin coating of PDMS and cure at 100 °C in oven, followed by optional heating in vacuum chamber depending on sample condition, and cutting; (c) release of specimens by dissolving the PAA in saline.

Table 1. Summary of thermal histories of PDMS samples tested.

Condition	Mix Ratio	Temperature Cured in Oven for 1 h	Post Processing Temperature in a Vacuum Chamber at 1 T for 1 h
A	10:1	100 °C	—
B	20:1	100 °C	—
C	20:1	100 °C	100 °C
D	20:1	100 °C	200 °C
E	20:1	100 °C	300 °C

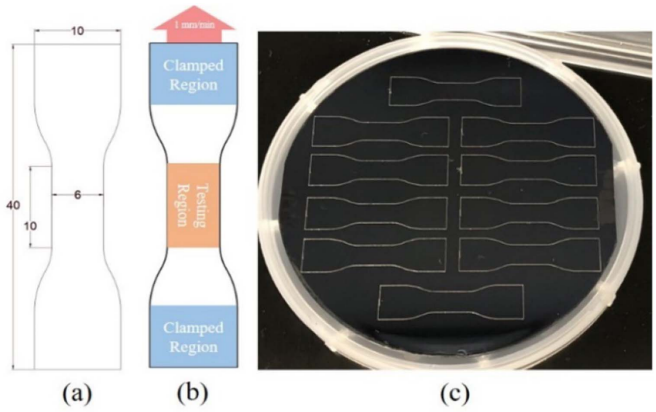

Figure 3. (a) Plan view of dog-bone specimen with units in mm. (b) Boundary conditions for testing the dog-bone specimens. (c) PDMS specimens on a 4″ diameter wafer after being cut with the Curio.

shown in figure 3. The dog-bone shape had a thin test section at the center, 10 mm long and 6 mm wide, with wider sections at the ends. The specimen was clamped in the tensile testing machine (Instron Model 5943, Norwood, MA) at the wide ends and stretched at a rate of 1 mm min^{-1}. Note that the dog-bone geometry helps minimize the effects from the clamps while maintaining uniform local stress and strain in the test section. The tensile test machine measured the displacement of the clamps throughout the test, which gives the global strain measurement.

To measure the local engineering strain in the test section, benchmarks on this region were manually tracked via image analysis (InfiniProbe TS-160, Infinity Photo Optical Co, Boulder CO, USA). The local strain was then analyzed for every 1 mm of global displacement and compared to the global strain measured by the apparatus. The relationship between the local and global strains is shown in figure 4, which relates the

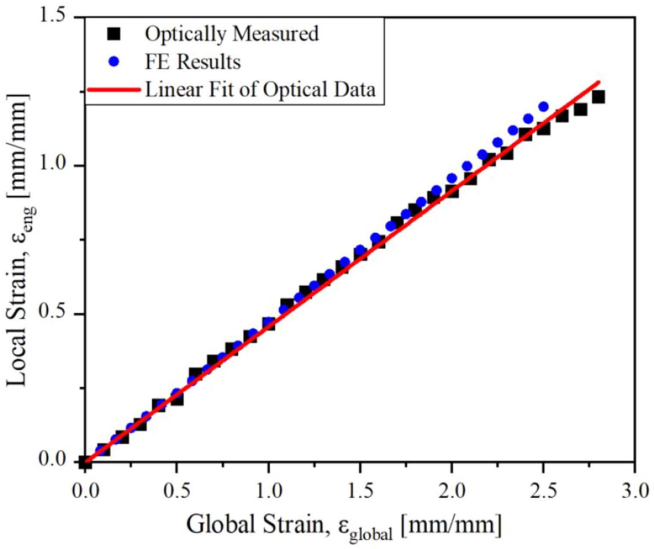

Figure 4. Local strain measured optically vs global strain measured from jaw displacement. The linear fit yields a correction factor of 0.458 for the modified type-C dumbbell sample shape.

local engineering strain ε_{eng} to the global engineering strain $\varepsilon_{\text{global}}$ via a correlation factor, m, as:

$$\varepsilon_{\text{eng}} = m\,\varepsilon_{\text{global}}. \tag{1}$$

From figure 4, the relation between ε_{eng} and $\varepsilon_{\text{global}}$ is linear with a correction factor, $m = 0.458$. A finite element (FE) analysis (ANSYS Inc, Canonsburg, PA) of the test geometry shown in figure 3 was performed to confirm the local to global strain conversion (see section S1 (stacks.iop.org/JMM/30/067001/mmedia) in supporting information for details of the FE model), which gave a correction factor, m_{FEA}, of 0.48, which is within 5% of that extracted from figure 4. The measured correction factor of 0.458 is thus used to calculate the engineering strain for all data presented in this work.

As discussed later, the Ogden hyperelastic material model [22, 31] was used to describe the behavior of the PDMS films in this work. The Ogden model utilizes a linear combination of the principle stretches λ_1, λ_2, and λ_3, instead of the stretch invariants used by other hyperelastic models, to simplify the strain energy function U to [22]:

$$U(\lambda_1, \lambda_2, \lambda_3) = \sum_{r=1}^{N} \frac{\mu_r}{\alpha_r}\left(\lambda_1^{\alpha_r} + \lambda_2^{\alpha_r} + \lambda_3^{\alpha_r} - 3\right). \tag{2}$$

where μ_r and α_r are material parameters. For incompressible solids the principle Cauchy stresses can be written as:

$$\sigma_i = \lambda_i \frac{\partial U}{\partial \lambda_i} - p \qquad (i = 1, 2, 3) \tag{3}$$

where p is an arbitrary hydrostatic pressure. For uniaxial tension tests, the principle stretch $\lambda_1 = \lambda$ is along the direction of stretching, and the corresponding principle Cauchy stress $\sigma_1 = \sigma$, and the other principle stresses $\sigma_2 = \sigma_3 = 0$. Additionally, the remaining principle stretches

$\lambda_2 = \lambda_3 = \lambda^{-1/2}$ due to the incompressibility constraint, and the arbitrary hydrostatic pressure is eliminated, and the following relationship is found by evaluating (3) with (2).

$$\sigma_{\text{eng}} = \frac{\sigma}{\lambda} = \sum_{r=1}^{N} \mu_r \left[\lambda^{\alpha_r - 1} - \lambda^{-(1+\frac{1}{2}\alpha_r)} \right]. \tag{4}$$

Since we wish to fit the Ogden model to our force and displacement data, which is accompanied by initial sample geometric measurements, the model should utilize the engineering stress and strain (σ_{eng}, ε_{eng}). The form of (4) provides that convenience by noticing that the stretch $\lambda = 1 + \varepsilon_{\text{eng}}$. In addition, the instantaneous shear modulus is given by the Ogden model to be:

$$G = \frac{1}{2} \sum_{r=1}^{N} \mu_r \alpha_r. \tag{5}$$

and the Young's (elastic) modulus is

$$E = 2G(1 + \nu) \tag{6}$$

where ν is Poisson's ratio, assumed to be 0.5 since PDMS has been shown to behave as an incompressible material [32]. The Young's modulus of PDMS is often reported in literature, though there is no specification in ASTM D412 for how to calculate the modulus for rubber-like materials. Specifying the linear region is thus determined by the tester, and there are reported elastic modulus values using data from 1% strain [17] all the way up to 40% strain [20] and even 100% strain [18] as the linear region. In the present work, we extract the elastic modulus as the slope of the linear fit of the data up to 5% engineering strain and the corresponding engineering stress and then compare that to the instantaneous elastic modulus from the fit of Ogden's hyperelastic model. A series of snapshots of the Condition-B PDMS sample being stretched in the Instron testing machine is shown in figure 5.

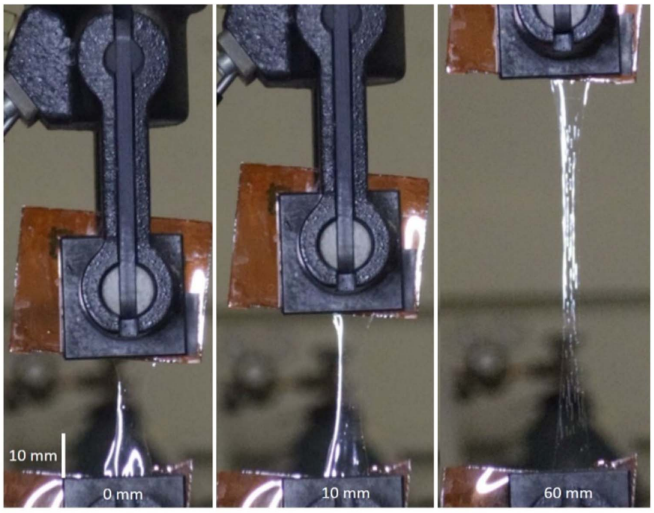

Figure 5. Sample of condition-B PDMS stretched at 0 mm, 10 mm, and 60 mm extension.

3. Results and discussion

The force-extension response of the PDMS films as measured by the jaw displacement of the Instron machine are shown in figure 5. The plots show classic hyperelastic behavior of the films for all the conditions tested in this work. The engineering stress–strain plots for the films after applying the correction factor as defined in (1) are shown in figure 6. It is clear that for all the cases, the average strain is higher than 100%. Further, the maximum engineering stress is a few MPa at failure. The box plots of the strain-to-failure and elastic modulus of the PDMS samples are plotted in figure 7. For 10:1 PDMS (Condition-A), the elastic modulus of 1.815 MPa is similar to that reported in literature [17, 28, 29]. For the 20:1 PDMS, however, the as-fabricated films (Condition-B) showed a softer film behavior with a modulus of 0.627 MPa, or 65% reduction compared to Condition-A. Further, the average strain to failure for the samples with Condition-B was about 300%, which indicates excellent stretchability. As the films were subjected to thermal histories of 100 °C, 200 °C, and 300 °C, however, the strain-to-failure reduced to 250%, 224%, and 106%, respectively, while the elastic modulus initially increased to 0.81 MPa, but then decreased to 0.71 MPa and 0.62 MPa, respectively. In fact, a 1 h extra time at 100 °C (Condition-B vs Condition-C) increases the stiffness by 30%. However, the stiffness values are still less than that for as-deposited PDMS with a 10:1 mixing ratio. One-way analysis of varaince (ANOVA) was performed for the resulting failure strain and elastic modulus and showed a statistically significant difference between the means of Conditions B through E for the failure strain (F (3, 12) = 35.1166, $p = 3.2 \times 10^{-6}$) and a lack of statistically significant difference for the elastic moduli (F (3, 12) = 1.9674, $p = 0.1728$). See section S3 of the Supporting Information.

The experimental data was then fit with the Ogden model described in section 2. It is noted that the data was also fit with the Mooney–Rivlin model, and the fits were compared with the Ogden model as described in the Supporting Information (section S2, figure S2, and table S1). This comparison, shown in table S1 of the Supporting Information, indicates that the Ogden Model fits the data with a higher correlation coefficient (R^2) compared to the Mooney–Rivlin model. Further, since the Ogden model can be a sum of infinite terms, the choice of the number of coefficients is usually left to the user [33]. In the present case, number of coefficient pairs (N) was chosen to be 2 as an increase in 'N' did not provide a significant improvement in the R^2 values.

Table 2 provides a summary of the values of modulus, failure strain, and the parameter fit with the Ogden model for all the conditions tested in this work. Figure 8 quantifies the Ogden $N = 2$ fit for one set of samples, illustrating its suitability. To satisfy kinematic requirements of the strain energy function, a necessary and sufficient condition on the coefficients is that $\alpha_i \mu_i > 0$. Furthermore it is common to require at least one set of coefficient pairs (α_i, μ_i) to be negative to

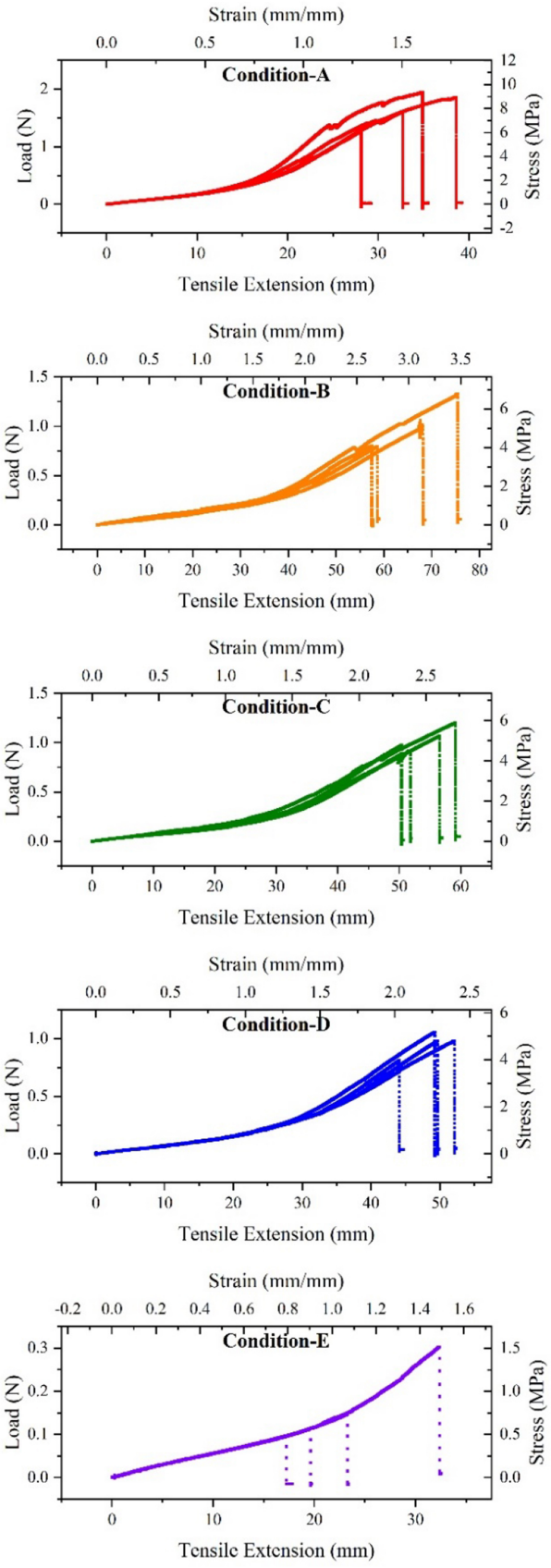

Figure 6. Raw data from instron tests given as load vs tensile extension (i.e. jaw displacement) with a sample size $n = 4$ for each condition. Engineering stress vs engineering strain plots for samples with different thermal histories as indicated in table 1.

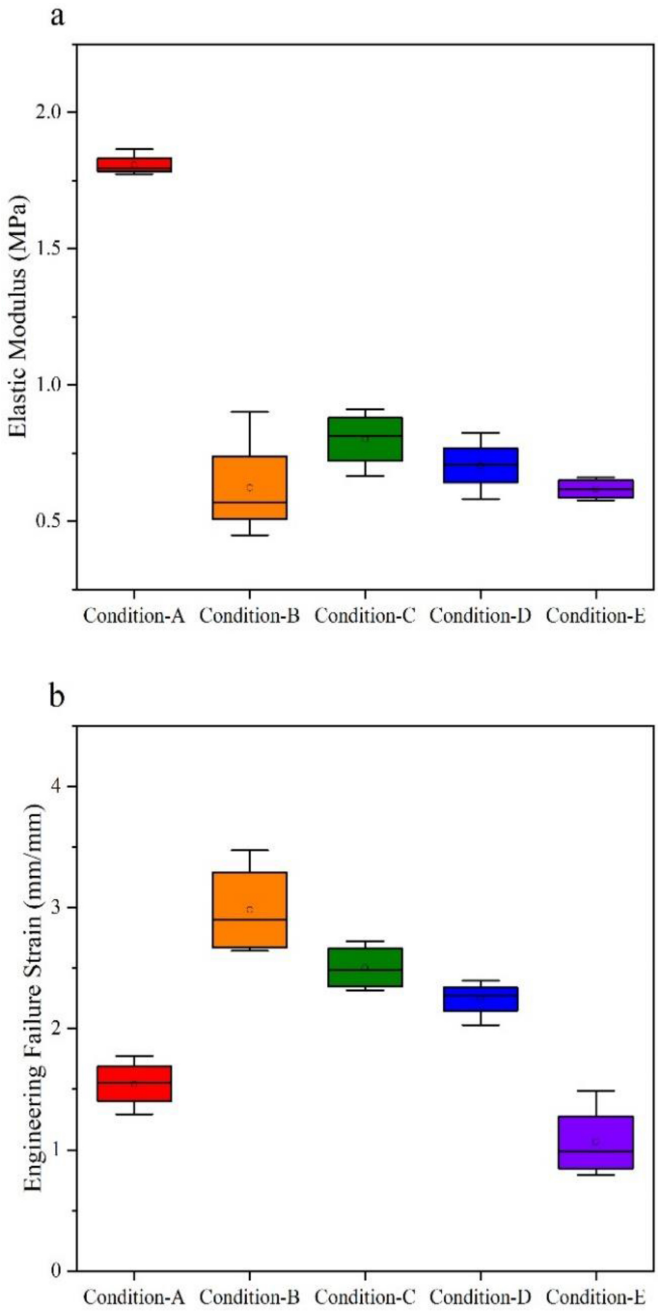

Figure 7. (a) Elastic modulus and (b) failure strain comparison for each condition tested.

capture characteristic behavior from other tests such as biaxial stress tests, and so the fit was performed holding the second coefficient pair (α_2, μ_2) to be negative for consistancy to previously reported data [22, 24].

While the Ogden model coefficients are largely phenomenological with no direct physical interpretation, there has been recent work linking the coefficients to physical parameters [31], one of which has been linked to the aging, or further crosslinking of the PDMS [24]. A consistent trend appears in each of the coefficients for the 20:1 samples cured under vacuum, with the α coefficients increasing and the μ coefficients decreasing with increasing thermal exposure. In

Table 2. Fit parameters for all test conditions with the R^2 for each fit. Shear modulus (G) and elastic modulus (E) are reported for the Ogden model, and the elastic modulus from the linear fit up to 5% strain is reported alongside for comparison.

	Elastic Modulus	Failure Strain	Ogden Constants					Ogden Model	
	E	ε_{eng}	α_1	α_2	μ_1	μ_2	R^2	G	E
Condition	(MPa)	(%)	(−)	(−)	(MPa)	(MPa)	(−)	(MPa)	(MPa)
A	1.815	154.5	5.030	0.000	0.214	0.000	0.9945	0.538	1.614
B	0.627	298.0	4.140	−1.259	0.065	−0.172	0.9988	0.244	0.732
C	0.805	250.3	4.541	−2.915	0.060	−0.122	0.9974	0.314	0.943
D	0.709	224.5	4.806	−1.131	0.053	−0.294	0.9997	0.292	0.877
E	0.621	106.3	5.888	−0.038	0.015	−12.441	0.9992	0.278	0.835

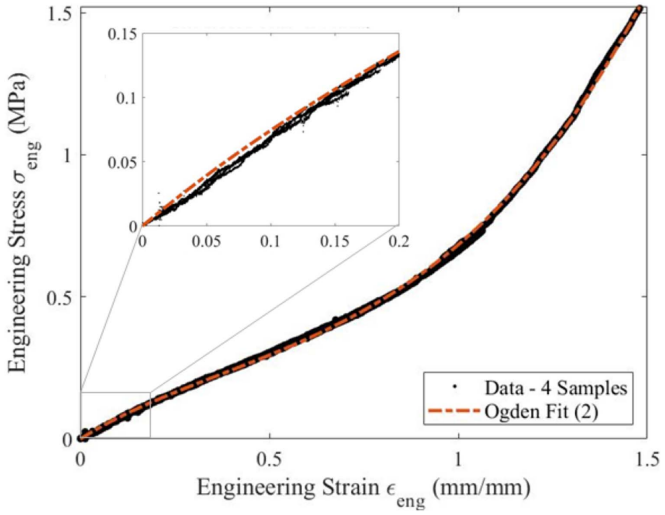

Figure 8. Ogden Fit (N = 2) to test data consisting of four samples of 20:1 PDMS cured at 300 °C (Condition-E).

addition, the coefficient pairs of the Ogden model conveniently sum together to give the instantaneous shear modulus as shown in (5). The elastic modulus resulting from the Ogden model matches the same decreasing trend found from the linear fit from the first 5% of strain. Hopf *et al* [24] suggest that crosslinking of the polymer chains is increased with aging and temperature, which is shown to increase the stiffness of PDMS. However, the results summarized in table 2 indicate a different trend, where increased exposure temperature softens the PDMS specimens. The authors speculate that the dominating effect responsible for this trend is increased thermal decomposition of the PDMS rather than increased crosslinking when the material is exposed to higher temperatures in vacuum.

4. Conclusions

The mechanical characteristics of 20:1 PDMS subjected to different thermal histories in a low vacuum environment were determined to quantify the effect of high-temperature heating cycles on PDMS properties. The results indicate that the PDMS maintained hyperelastic behavior under all the conditions evaluated the paper. As the post-cure heating temperature increased from 100 °C to 300 °C, the modulus decreased from 0.805 MPa to 0.621 MPa, while the failure strain decreased from 250% to 106%. The high stretchability maintained by PDMS shows only a limited degradation of its properties upon thermal exposure. The softening of the PDMS on heating indicates that polymer chain degradation rather than crosslinking occurs at temperatures up to 300 °C. The stress–strain response of the films is represented by a second-order Ogden hyperelastic model. The results indicate suitability of PDMS as a substrate material for microelectronics fabrication processes for temperatures up to 300 °C and the importance of mixing ratio. Increasing the cross-linker increases the deterioration and reduces the elastic modulus of PDMS.

The results presented in this paper indicate that the 20:1 PDMS maintained suitable mechanical properties through high-temperature treatment including maintaining significant film stretchability. Further tests such as biaxial stretch, and fatigue testing are a subject of future work to more fully characterize the mechanical response of PDMS subjected to high-temperatures.

Acknowledgments

The authors gratefully acknowledge research funding from Highmark Health.

ORCID iDs

Derya Z Tansel https://orcid.org/0000-0003-0636-7797
Jacob Brenneman https://orcid.org/0000-0003-4786-4466
Gary K Fedder https://orcid.org/0000-0002-2380-5210
Rahul Panat https://orcid.org/0000-0002-4824-2936

References

[1] Belanger M C and Marois Y 2001 Hemocompatibility, biocompatibility, inflammatory and in vivo studies of primary reference materials low-density polyethylene and polydimethylsiloxane: a review *J. Biomed. Mater. Res.* **58** 467–77
[2] Eduok U, Faye O and Szpunar J 2017 Recent developments and applications of protective silicone coatings: a review of PDMS functional materials *Prog. Org. Coat.* **111** 124–63
[3] Wang X, Liu Z and Zhang T 2017 Flexible sensing electronics for wearable/attachable health monitoring *Small* **13** 1602790

[4] Dutta I and Panat R 2017 Highly stretchable interconnect devices and systems United States of America Patent 9770759

[5] Arafat Y, Dutta I and Panat R 2015 Super-stretchable metallic interconnects on polymer with a linear strain of up to 100% *Appl. Phys. Lett.* **107** 081906

[6] Arumugam V, Naresh M D and Sanjeevi R 1994 Effect of strain-rate on the fracture-behavior of skin *J. Biosci.* **19** 307–13

[7] Wang Z, Volinsky A A and Gallant N D 2014 Crosslinking effect on polydimethylsiloxane elastic modulus measured by custom-built compression instrument *J. Appl. Polym. Sci.* **131** 41050

[8] Saleh M S, HamidVishkasougheh M, Zbib H and Panat R 2018 Polycrystalline micropillars by a novel 3-D printing method and their behavior under compressive loads *Scr. Mater.* **149** 144–9

[9] Kim D, Jeong S, Moon J and Kang K 2006 Ink-jet printing of silver conductive tracks on flexible substrates *Mol. Cryst. Liq. Cryst.* **459** 45/[325]–55/[35]

[10] Saleh M S, Hu C and Panat R 2017 Three-dimensional microarchitected materials and devices using nanoparticle assembly by pointwise spatial printing *Sci. Adv.* **3** e1601986

[11] Rahman T, Renaud L, Heo D, Renn M J and Panat R 2015 Aerosol based direct-write micro-additive fabrication method for sub-mm 3D metal-dielectric structures *J. Micromech. Microeng.* **25** 107002

[12] Rahman M T, McCloy J, Ramana C V and Panat R 2016 Structure, electrical characteristics, and high-temperature stability of aerosol jet printed silver nanoparticle films *J. Appl. Phys.* **120** 075305

[13] Danaei R, Varghese T, Ahmadzadeh M, McCloy J, Hollar C, Sadeq Saleh M, Park J, Zhang Y and Panat R 2019 Ultrafast fabrication of thermoelectric films by pulsed light sintering of colloidal nanoparticles on flexible and rigid substrates *Adv. Eng. Mater.* **21** 1800800

[14] Rahman M T, Cheng C-Y, Karagoz B, Renn M, Schrandt M, Gellman A and Panat R 2019 High performance flexible temperature sensors via nanoparticle printing *ACS Appl. Nano Mater.* **2** 3280–91

[15] Grassie N and Macfarlane I G 1978 The thermal degradation of polysiloxanes—I. Poly(dimethylsiloxane) *Eur. Polym. J.* **14** 875–84

[16] Camino G, Lomakin S M and Lazzari M 2001 Polydimethylsiloxane thermal degradation part 1. Kinetic aspects *Polymer* **42** 2395–402

[17] Liu M, Sun J and Chen Q 2009 Influences of heating temperature on mechanical properties of polydimethylsiloxane *Sens. Actuators A: Phys.* **151** 42–45

[18] Khanafer K, Duprey A, Schlicht M and Berguer R 2009 Effects of strain rate, mixing ratio, and stress–strain definition on the mechanical behavior of the polydimethylsiloxane (PDMS) material as related to its biological applications *Biomed. Microdevices* **11** 503–8

[19] Liu M 2007 Characterization study of bonded and unbonded polydimethylsiloxane aimed for bio-micro-electromechanical systems-related applications *J. Micro/Nanolithogr. MEMS MOEMS* **6** 023008

[20] Johnston I D, McCluskey D K, Ck L T and Tracey M C 2014 Mechanical characterization of bulk Sylgard 184 for microfluidics and microengineering *J. Micromech. Microeng.* **24**

[21] Schneider F, Fellner T, Wilde J and Wallrabe U 2008 Mechanical properties of silicones for MEMS *J. Micromech. Microeng.* **18**

[22] Ogden R W 1972 Large deformation isotropic elasticity—on the correlation of theory and experiment for incompressible rubberlike solids *Proc. R. Soc. A: Math. Phys. Eng. Sci.* **326** 565–84

[23] Mooney M 1940 A theory of large elastic deformation *J. Appl. Phys.* **11** 582–92

[24] Hopf R, Bernardi L, Menze J, Zundel M, Mazza E and Ehret A E 2016 Experimental and theoretical analyses of the age-dependent large-strain behavior of Sylgard 184 (10:1) silicone elastomer *J. Mech. Behav. Biomed. Mater.* **60** 425–37

[25] Kim T K, Kim J K and Jeong O C 2011 Measurement of nonlinear mechanical properties of PDMS elastomer *Microelectron. Eng.* **88** 1982–5

[26] Rivlin R 1948 Large elastic deformations of isotropic materials. I. Fundamental concepts *Philos. Trans. R. Soc. London Ser. A: Math. Phys. Sci.* **240** 459–90

[27] Yeoh O H 1990 Characterization of elastic properties of carbon-black-filled rubber vulcanizates *Rubber Chem. Technol.* **63** 792–805

[28] Sharfeddin A, Volinsky A A, Mohan G and Gallant N D 2015 Comparison of the macroscale and microscale tests for measuring elastic properties of polydimethylsiloxane *J. Appl. Polym. Sci.* **132**

[29] Liu M, Sun J, Sun Y, Bock C and Chen Q 2009 Thickness-dependent mechanical properties of polydimethylsiloxane membranes *J. Micromech. Microeng.* **19**

[30] ASTM 2016 Standard test methods for vulcanized rubber and thermoplastic elastomers—tension *100 Barr Harbor Drive, PO Box C700, West Conshohocken, PA 19428-2959* (United States: ASTM International)

[31] Ehret A E 2015 On a molecular statistical basis for Ogden's model of rubber elasticity *J. Mech. Phys. Solids* **78** 249–68

[32] Bernardi L, Hopf R, Ferrari A, Ehret A E and Mazza E 2017 On the large strain deformation behavior of silicone-based elastomers for biomedical applications *Polym. Test.* **58** 189–98

[33] Kim B, Lee S B, Lee J, Cho S, Park H, Yeom S and Park S H 2012 A comparison among neo-Hookean model, Mooney–Rivlin model, and Ogden model for chloroprene rubber *Int. J. Precis. Eng. Manuf.* **13** 759–64